Supporting Information for

Determinants of regioselectivity of heterostructures in cation exchange reactions

Xuelian Qu,[a‡] Huisheng Zhang,[b‡] Tianyi Gao,[a] Fei Zhang,[a] Ying Zhang,[a] Dingjiang Xue,[c] and Yang Liu[a*]

[a]Department of Materials Science, Fudan University, Shanghai 200433, China.

[b]Research Institute of Materials Science of Shanxi Normal University & Key Laboratory of Magnetic Molecules and Magnetic Information Materials of Ministry of Education, Taiyuan 030031, China.

[c]Beijing National Laboratory for Molecular Sciences (BNLMS), CAS Key Laboratory of Molecular Nanostructure and Nanotechnology, Institute of Chemistry, Chinese Academy of Sciences, Beijing 100190, China; University of Chinese Academy of Sciences, Beijing 100049, China

Materials and Methods

Materials. All chemicals were used as received without further purification. Copper(I) thiocyanate (CuSCN, 99%), Indium chloride ($InCl_3$, 98%), zinc chloride ($ZnCl_2$, ≥ 97%), cadmium acetate dihydrate ($Cd(OAc)_2 \cdot 2H_2O$), oleylamine (OAm, 70%), 1-octadecene (ODE, 90%), benzyl ether (98%) and trioctylphosphine (TOP, technical grade, 90%) were purchased from Sigma-Aldrich.

Synthesis of $Cu_{1.81}S$ Template Nanoplates. The synthesis of roxbyite $Cu_{1.81}S$ nanoplates was adapted from a previously reported method with modifications.[1] In a typical reaction, 60 mg CuSCN and 15 mL OAm were loaded in a three-neck flask. The reaction mixture was evacuated at 100 °C for 30 min before refill with N_2. Then, the mixture was heated to 240 °C and the reaction was maintained at this temperature for 30 min before air-cooled to room temperature. After the reaction completed, 10 mL of isopropanol was added into the crude reaction mixture, followed by centrifuging at 4000 rpm for 2 min. The precipitates were redispersed in 10 mL of hexane, then 10 mL of isopropanol was added. A second round of centrifugation was carried out at 4000 rpm for 2 min to remove excess ligands and impurities. The products were finally dispersed in hexane. The purification process was applied to all the NCs described in this work.

Synthesis of $Cu_{1.81}S@CuInS_2$ heterostructures. The synthesis of $Cu_{1.81}S@CuInS_2$ heterostructures was adapted from a previously reported method with modifications.[2] In a typical reaction, the In-TOP precursor was prepared by dissolving 22 mg (0.1 mmol) of $InCl_3$ in 0.5 mL of TOP and 2.5 mL of ODE by brief sonication. In a separate vial, the $Cu_{1.81}S$ nanoplates dispersion was prepared by dispersing a batch of dry $Cu_{1.81}S$ nanoplates (typically ~70 mg) in 2 mL of OAm by brief sonication. The dispersion was mixed with 8 mL ODE and heated at 55 °C under vacuum for 30 min. After refilling the flask with N_2, In-TOP precursor was dropwise injected into the mixture containing $Cu_{1.81}S$ nanoplates using a syringe pump at the rate of 2 mL/h. To collect the NCs, 10 mL of ethanol was added when injection completed, followed by centrifuging at 4000 rpm for 2 min.

Synthesis of $Cu_{1.81}S$/ZnS and $Cu_{1.81}S$/CdS heterostructures. The synthesis of $Cu_{1.81}S$/ZnS and $Cu_{1.81}S$/CdS heterostructures was adapted from a previously reported method with modifications.[3] In a typical reaction, a mixture of 250 mg $ZnCl_2$ (or 245 mg $Cd(OAc)_2 \cdot 2H_2O$) and 8 mL of OAm, 2 mL of ODE and 15 mL benzyl ether was heated at 100 °C under vacuum for 30 min. After refilling the flask with N_2, the mixture was heated to 180 °C (or 100 °C for Cd-exchange) for 30 min before air-cooled to 55 °C. In a separate vial, $Cu_{1.81}S$ dispersion was prepared by dispersing 6 mg dry $Cu_{1.81}S$ nanoplates in 3 mL of TOP by brief sonication, and the dispersion was injected into the reaction flask. After keeping the reaction mixture at 55 °C for 60 min (55 °C for 1.5 min for $Cu_{1.81}S$/CdS heterostructures and 100 °C for 30 min for complete CdS nanoplates), the products were isolated by ethanol precipitation and centrifugation at 4000 rpm for 2 min.

CE of $Cu_{1.81}S$-based heterostructures with Zn^{2+}, Cd^{2+}, and In^{3+} at 55 °C. In a typical reaction of $Cu_{1.81}S$@$CuInS_2$, a mixture of 250 mg of $ZnCl_2$ (or 245 mg of $Cd(OAc)_2 \cdot 2H_2O$), 8 mL of OAm, 2 mL of ODE and 15 mL benzyl ether was heated at 100 °C under vacuum for 30 min. After refilling the flask with N_2, the mixture was heated to 180 °C (or 100 °C for Cd-exchange) for 30 min before air-cooled to 55 °C. In a separate vial, the $Cu_{1.81}S$@$CuInS_2$ dispersion was prepared by dispersing 10 mg dry NCs in 3 mL of TOP by brief sonication, and the dispersion was injected into the reaction flask. After keeping the reaction mixture at 55 °C for 30 min, the products were isolated by ethanol precipitation and centrifugation at 4000 rpm for 2 min. Similarly, the In^{3+} exchange reactions on $Cu_{1.81}S$/ZnS or $Cu_{1.81}S$/CdS used 220 mg of $InCl_3$ as In precursor while other parameters remain unchanged.

CE of $Cu_{1.81}S$-based heterostructures with Zn^{2+}, Cd^{2+}, and In^{3+} at 155 °C. In a typical reaction, a mixture of 45 mg of $ZnCl_2$ (or 40 mg of $Cd(OAc)_2 \cdot 2H_2O$) and 5 mL of OAm was heated at 100 °C under vacuum for 30 min. After refilling the flask with N_2, mixture was heated to 155°C for 30 min. In a separate vial, the $Cu_{1.81}S$@$CuInS_2$ dispersion was prepared by dispersing 10 mg dry NCs

in 2.5 mL of TOP by brief sonication, and the dispersion was injected into the reaction flask. After keeping the reaction mixture at 155 °C for 30 min, the products were isolated by ethanol precipitation and centrifugation at 4000 rpm for 2 min. Similarly, the In^{3+} exchange reactions on $Cu_{1.81}S$/ZnS or $Cu_{1.81}S$/CdS used 55 mg of $InCl_3$ as In precursor and a batch of dry $Cu_{1.81}S$/ZnS or $Cu_{1.81}S$/CdS nanoplates (typically ~6 mg) while other parameters remain unchanged.

Characterization. TEM and HRTEM images were obtained using a JEOL JEM-2010 at an accelerating voltage of 200 kV. HAADF-STEM images, AC-STEM images, and STEM-EDS maps were collected using a JEOL JEMARM200F STEM equipped with spherical aberration correctors on the image, at an accelerating voltage of 200 kV. TEM grids were prepared by dropping a dilute NC dispersion onto a carbon-coated copper or gold TEM grid and allowing the sample to dry under air. Powder X-ray diffraction (XRD) measurements were carried out using a Bruker D8 Advance diffractometer with a Cu Kα X-ray source. Samples for XRD were prepared by drop-casting concentrated NC dispersions onto glass slides.

Density functional theory (DFT) calculations. Density-functional theory (DFT) calculations were performed using the projector augmented wave (PAW) method[4] implemented with the Vienna ab initio simulation package (VASP)[5]. The Perdew−Burke−Ernzerhof (PBE) approximation was used to describe the exchange and correlation functionals[6]. The plane-wave cutoff energy was set to 400 eV, the Hellmann−Feynman force on each atom was smaller than 0.01 eV $Å^{-1}$, and the total energy converged to 10^{-5} eV for structural optimization. $Cu_{1.81}S$ and $CuInS_2$ (CdS, ZnS) were modeled by a 1 × 1 and 2 × 2 supercell, respectively. A vacuum space of 15 Å was added between adjacent supercells. The 6 × 6 × 1 and 12 × 12 × 1 gamma-centered Monkhorst-Pack *k*-point mesh were used for $Cu_{1.81}S$ and $CuInS_2$ (CdS, ZnS), respectively. We used heat of reaction ($^{\Delta_r E}$) to estimate the possibility of occurrence of the CE reactions. DFT calculations were performed to assess the heat of reaction for CE reactions on (800) and (080) planes of $Cu_{1.81}S$ and (001) and (010) planes of $CuInS_2$ (CdS, ZnS). Our DFT calculations were based on the projector augmented

wave (PAW) method[4] implemented using the Vienna ab initio simulation package (VASP)[5]. The Perdew-Burke-Ernzerhof (PBE) approximation was used to describe the exchange and correlation functionals[6]. The plane-wave cutoff energy was set to 400 eV, the Hellmann-Feynman force on each atom was smaller than 0.01 eV $Å^{-1}$, and the total energy converged to 10^{-5} eV for structural optimization. $Cu_{1.81}S$ and $CuInS_2$ (CdS, ZnS) were modelled by a 1 × 1 and 2 × 2 supercell, respectively. A vacuum space of 15 Å was added between adjacent supercells. Atoms of the upper two layers were allowed to relax while those of the lower layers were fixed at their bulk positions. The 6 × 6 × 1 and 12 × 12 × 1 gamma-centered Monkhorst-Pack *k*-point mesh were used for $Cu_{1.81}S$ and $CuInS_2$ (CdS, ZnS), respectively. The DFT calculations of CE reactions are divided into the following three groups:

1. As shown in Figure S8, hexagonal $Cu_{1.81}S$ nanoplates expose their (800) and (080) planes. $Cu_{1.81}S$ adopts a *hcp*-type of unit cell with 8 layers of atoms along its *a*- and *b*-axis. For computational efficiency, we focused on layer 1 and layer 5 of (800) planes (denoted as layer A1 and layer A5) as well as layer 1 and layer 5 of (080) planes (denoted as layer B1 and layer B5) (Figure S2,S3) in the following calculations as they exhibit the maximal and minimal planar density of Cu atom in the (800) and (080) planes, respectively. On one hand, we placed an In atom in layer A1 (with the highest Cu planar density) by substituting the nearest three Cu atoms for charge neutralization. On the other hand, an In atom was placed in layer A5 (with the lowest Cu planar density) by removing three loosely packed Cu atoms. The $\Delta_r E$ for In exchanges Cu in $Cu_{1.81}S$ can be described as:

$$\Delta_r E = (E_{Cu_{55}InS_{32}} + 3E_{Cu}) - (E_{Cu_{58}S_{32}} + E_{In})$$

where $E_{cu_{58}S_{32}}$, $E_{cu_{55}InS_{32}}$, E_{In}, E_{Cu} are the total energy of $Cu_{58}S_{32}$ ($Cu_{1.81}S$), In exchanged $Cu_{1.81}S$, In, and Cu atom, respectively. The $\Delta_r E$ values shown in Table S1 and Fig. 1 are averaged from different layers. The $\Delta_r E$ values for Cd and Zn exchange Cu in $Cu_{1.81}S$ follows similar calculations except for divalent charge compensation.

2. In contrast to $Cu_{1.81}S$, all cations in wurtzite $CuInS_2$ (CdS, ZnS) are equivalent. The Cu and In atoms in the wurtzite structure of $CuInS_2$ share the same positions with half occupancies. For computational convenience, we alternately assigned the cation site as Cu and In atoms with full occupancies. The Cd (or Zn) exchange Cu and In in $CuInS_2$ can be described as two Cd (or Zn) atoms substituting a pair of Cu and In atoms. The $\Delta_r E$ for Cd exchange Cu and In in $CuInS_2$ can be described as:

$$\Delta_r E = (E_{Cu_{19}In_{19}Cd_2S_{40}} + E_{Cu} + E_{In}) - (E_{Cu_{20}In_{20}S_{40}} + 2E_{Cd})$$

where $E_{Cu_{20}In_{20}S_{40}}$, $E_{Cu_{19}In_{19}Cd_2S_{40}}$, E_{In}, E_{Cu}, E_{Cd} are the total energy of $E_{Cu_{20}In_{20}S_{40}}$ ($CuInS_2$), Cd exchanged $CuInS_2$, In, Cu, and Cd atom, respectively. The $\Delta_r E$ values for Zn exchanges Cu and In in $CuInS_2$ follows similar calculations except for using Zn atoms.

3. Colloidal synthesis of In_2S_3 through the exchange of Cd (or Zn) with In in the CdS (or ZnS) unit cell is challenging due to the thermodynamic preference of In_2S_3 for adopting the trigonal (γ-In_2S_3) or tetragonal (β-In_2S_3) polymorph[7], rather than hexagonal (wurtzite) or cubic (zincblende) phase. Previous reports have shown that In can replace Cd or Zn in CdO,[8] ZnO,[9] CdS[10] and ZnS[11] nanocrystals (NCs) without changing the template crystal structure. Additionally, In can be doped into CdO/ZnO structures by substituting equimolar Cd/Zn from host lattices, producing an increased electron density in the doped NCs.[12] Therefore, in this study, the exchange of Cd (or Zn) with In was described as the replacement of one Cd/Zn atom with one In atom in the calculation of $\Delta_r E$. The $\Delta_r E$ for In exchange Cd in CdS can be described as:

$$\Delta_r E = (E_{Cd_{15}InS_{16}} + E_{Cd}) - (E_{Cd_{16}S_{16}} + E_{In})$$

where $E_{Cd_{40}S_{40}}$, $E_{Cd_{39}InS_{40}}$, E_{In}, E_{Cd} are the total energy of $E_{Cd_{40}S_{40}}$ (CdS), In exchanged CdS, In, and Cd atom, respectively. The $\Delta_r E$ for In exchange Zn in ZnS follows similar calculations except for using ZnS.

Table S1. Summary of heat of reaction $\Delta_r E$ per foreign atom on $Cu_{1.81}S$, CdS, ZnS, $CuInS_2$ based on DFT calculations.

host lattice	foreign atom	crystal planes	$\Delta_r E$ (eV)	ΔE (eV)
$Cu_{1.81}S$	Zn	(100)	-0.534	0.084
		(010)	-0.618	
	Cd	(100)	-0.669	0.245
		(010)	-0.914	
	In	(100)	-0.877	0.534
		(010)	-1.411	
$CuInS_2$	Zn	(001)	-0.587	0.626
		(010)	-1.213	
	Cd	(001)	-0.738	0.333
		(010)	-1.071	
ZnS	In	(001)	-0.125	0.261
		(010)	-0.386	
CdS	In	(001)	-0.089	0.132
		(010)	-0.221	

Table S2. The calculated ELF values and the corresponding reactions.

Ref	Reaction	Calculated ELF values			
Fig. 1b	Zn→$CuInS_2$	*n(*Zn)=0.47	*n(*In)=0.01	*n(*Cu)=0.03	*n(*S)=0.82
Fig. 1c	Zn→$CuInS_2$	*n(*Zn)=0.96	*n(*In)=0.15	*n(*Cu)=0.21	*n(*S)=0.76
Fig. 1d	In→ZnS	*n(*Zn)=0.22	*n(*In)=0.45		*n(*S)=0.82
Fig. 1e	In→ZnS	*n(*Zn)=0.13	*n(*In)=0.84		*n(*S)=0.75
Fig. S7a	Cd→$CuInS_2$	*n(*Cd)=0.77	*n(*In)=0.02	*n(*Cu)=0.03	*n(*S)=0.72
Fig. S7b	Cd→$CuInS_2$	*n(*Cd)=0.98	*n(*In)=0.21	*n(*Cu)=0.26	*n(*S)=0.81
Fig. S7c	In→CdS	*n(*Cd)=0.29	*n(*In)=0.37		*n(*S)=0.84
Fig. S7d	In→CdS	*n(*Cd)=0.26	*n(*In)=0.94		*n(*S)=0.66

Table S3. Crystallographic data and calculated lattice mismatch between $Cu_{1.81}S$ template and product metal sulfides.

	$Cu_{1.81}S$	CdS	ZnS	$CuInS_2$
Space group	*p1*	*p63mc*	*p63mc*	*p63mc*
a (Å)	13.409	4.150	3.800	3.897
b (Å)	13.405	4.150	3.800	3.897
c (Å)	15.485	6.737	6.230	6.441
α (°)	90.022	90.000	90.000	90.000
β (°)	90.021	90.000	90.000	90.000
γ (°)	90.020	120.000	120.000	120.000
lattice misfit, ε_a	--	+7.2%	-1.8%	+0.67%
lattice misfit, ε_c	--	+0.48%	-7.1%	-3.9%

Note:

The lattice misfit between CdS and $Cu_{1.81}S$ along *c*-axis (edge direction of nanoplate) of $Cu_{1.81}S$ can be calculated as: $\varepsilon_{a}^{CdS} = \frac{4d_{a}^{CdS}}{d_{c}^{Cu1.81S}} - 1$, where d_{a}^{CdS} is the lattice parameter of the CdS unit cell along its *a*-axis; $d_{c}^{Cu1.81S}$ is the lattice parameter of the $Cu_{1.81}S$ unit cell along its *c*-axis.

The lattice misfit between CdS and $Cu_{1.81}S$ along *a*-axis (thickness direction of nanoplate) of $Cu_{1.81}S$ can be calculated as: $\varepsilon_{c}^{CdS} = \frac{2d_{c}^{CdS}}{d_{a}^{Cu1.81S}} - 1$, where d_{c}^{CdS} is the lattice parameter of the CdS unit cell along its *c*-axis; $d_{a}^{Cu1.81S}$ is the lattice parameter of the $Cu_{1.81}S$ unit cell along its *a*-axis.

The lattice mismatch between $Cu_{1.81}S$ and other product metal sulfides are calculated using the same method.

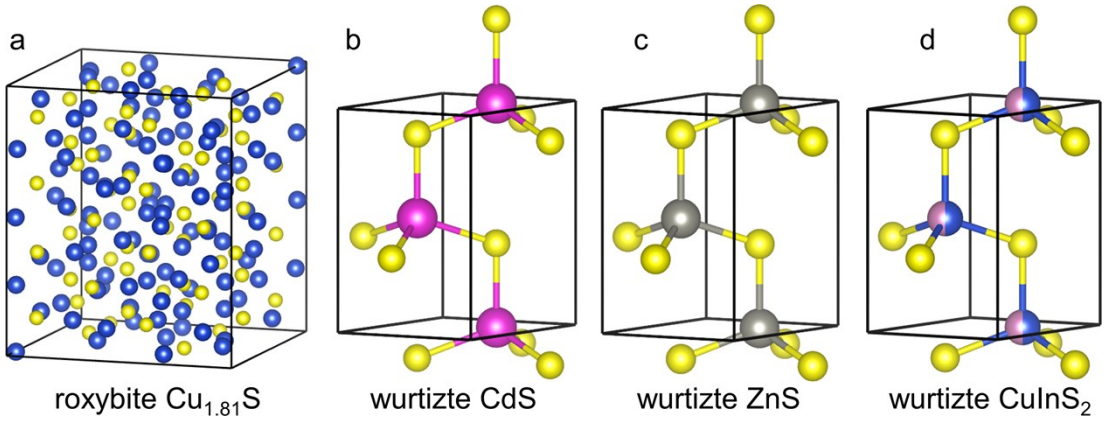

Fig. S1. Crystal structure models of (a) roxbyite $Cu_{1.81}S$, (b) wurtzite CdS, (c) wurtzite ZnS, and (d) wurtzite $CuInS_2$. The black lines depict the unit cell of each crystal structure.

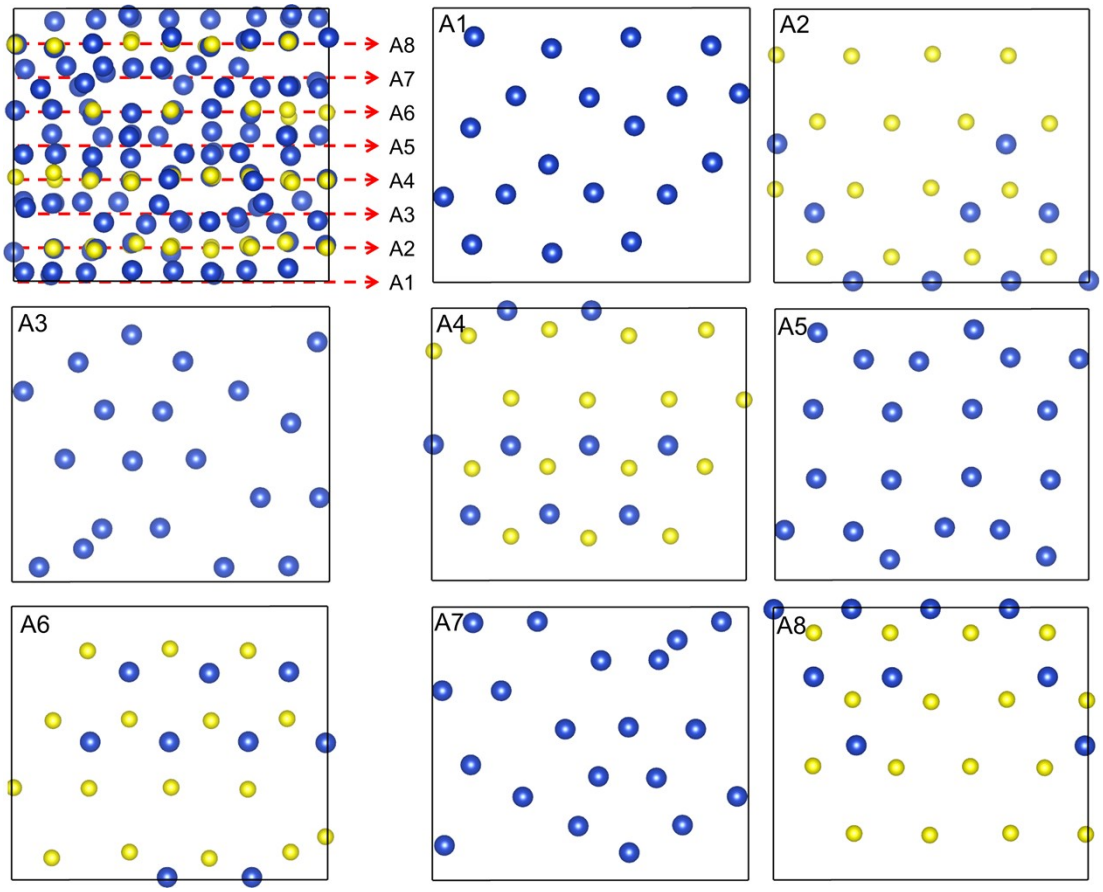

Fig. S2. The top-left panel shows the crystal structure model of roxbyite $Cu_{1.81}S$ viewing along [010] direction. Panels A1~A8 show eight (100) planes (viewing along [100] direction) of the unit cell, where sulfur atoms are hexagonally packed. The blue and yellow balls represent copper and sulfur atoms, respectively. The black lines depict the $Cu_{1.81}S$ unit cell.

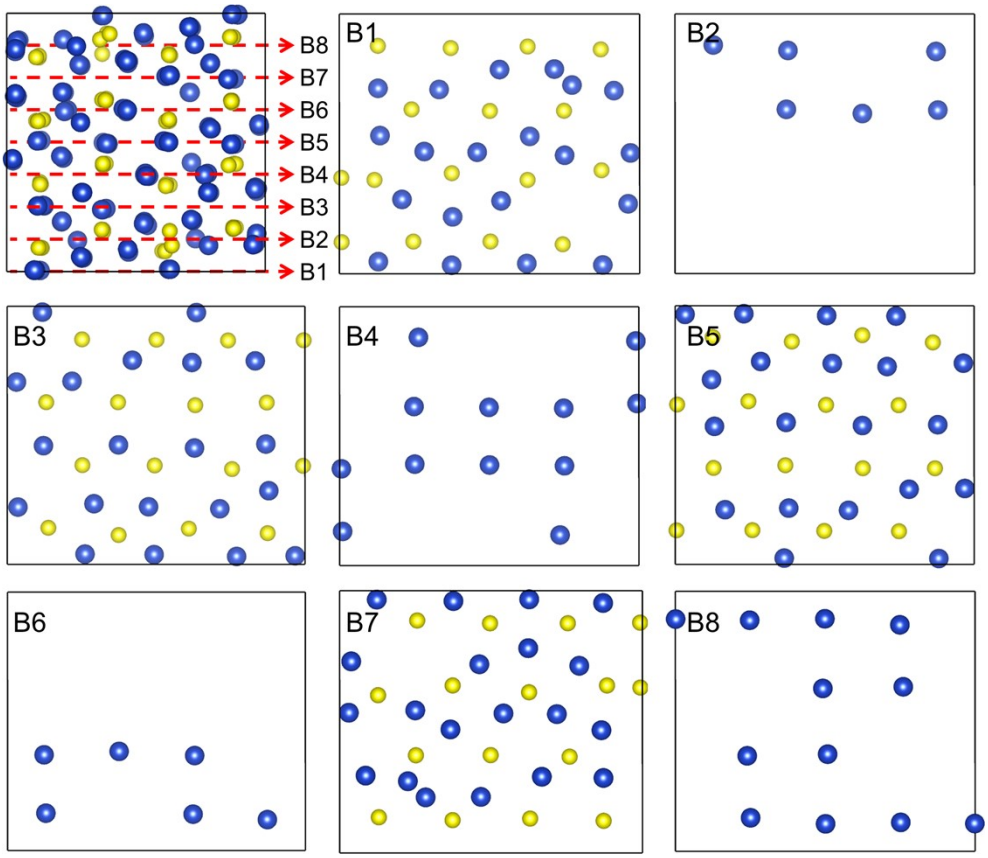

Fig. S3. The top-left panel shows the crystal structure model of roxbyite $Cu_{1.81}S$ viewing along [001] direction. Panels B1~B8 show eight (010) planes (viewing along [010] direction) of the unit cell, where sulfur atoms are hexagonally packed. The blue and yellow balls represent copper and sulfur atoms, respectively. The black lines depict the $Cu_{1.81}S$ unit cell.

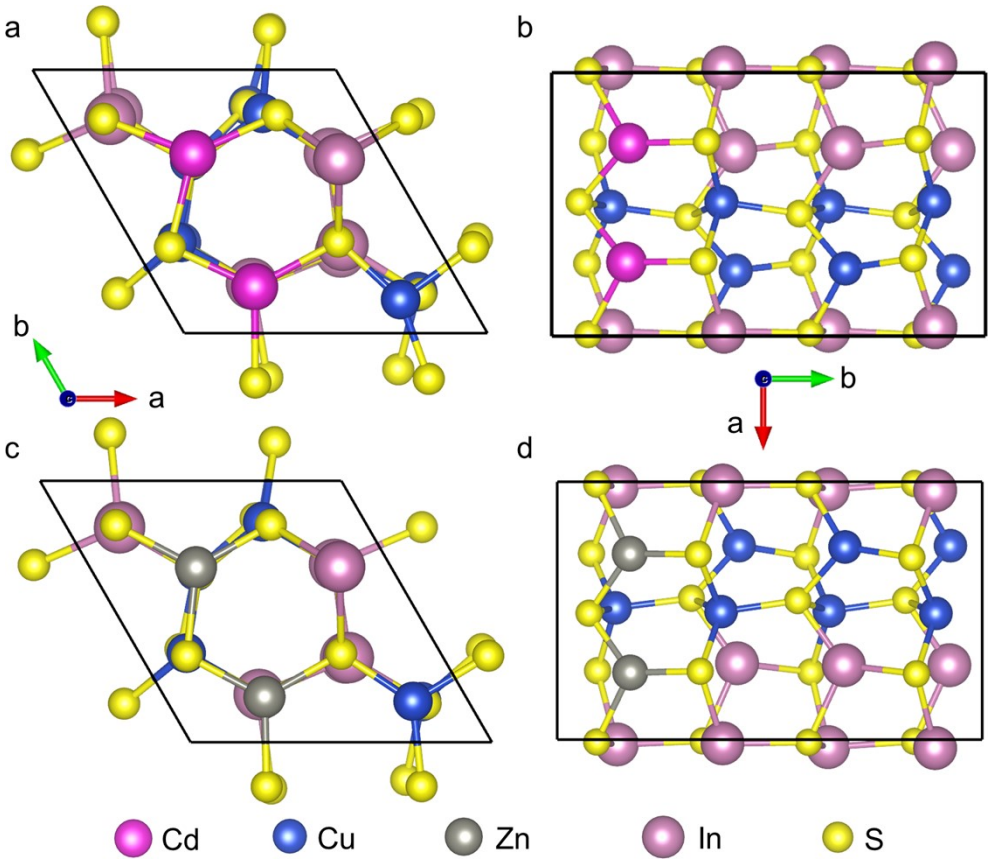

Fig. S4. The relaxed models for (a,b) Cd→$CuInS_2$ and (c,d) Zn→$CuInS_2$ reactions viewing along different directions. The black lines depict the unit cell of each crystal structure.

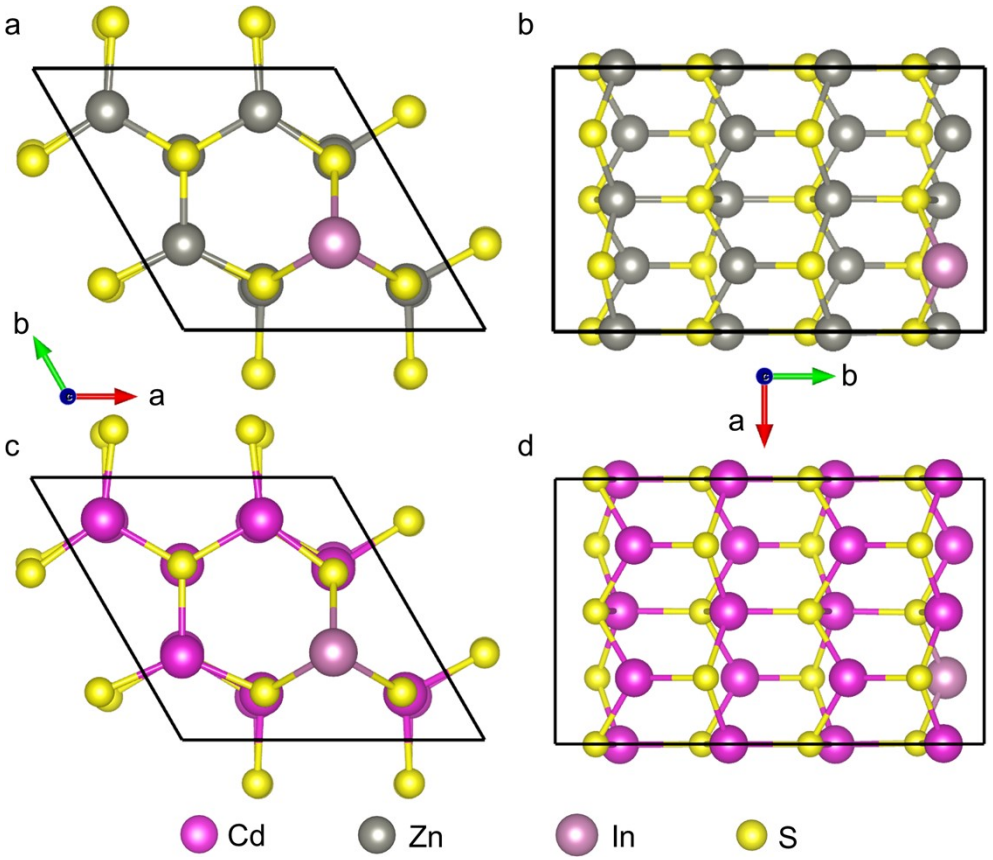

Fig. S5. The relaxed models for (a,b) In→ZnS and (c,d) In→CdS reactions viewing along different directions. The black lines depict the unit cell of each crystal structure.

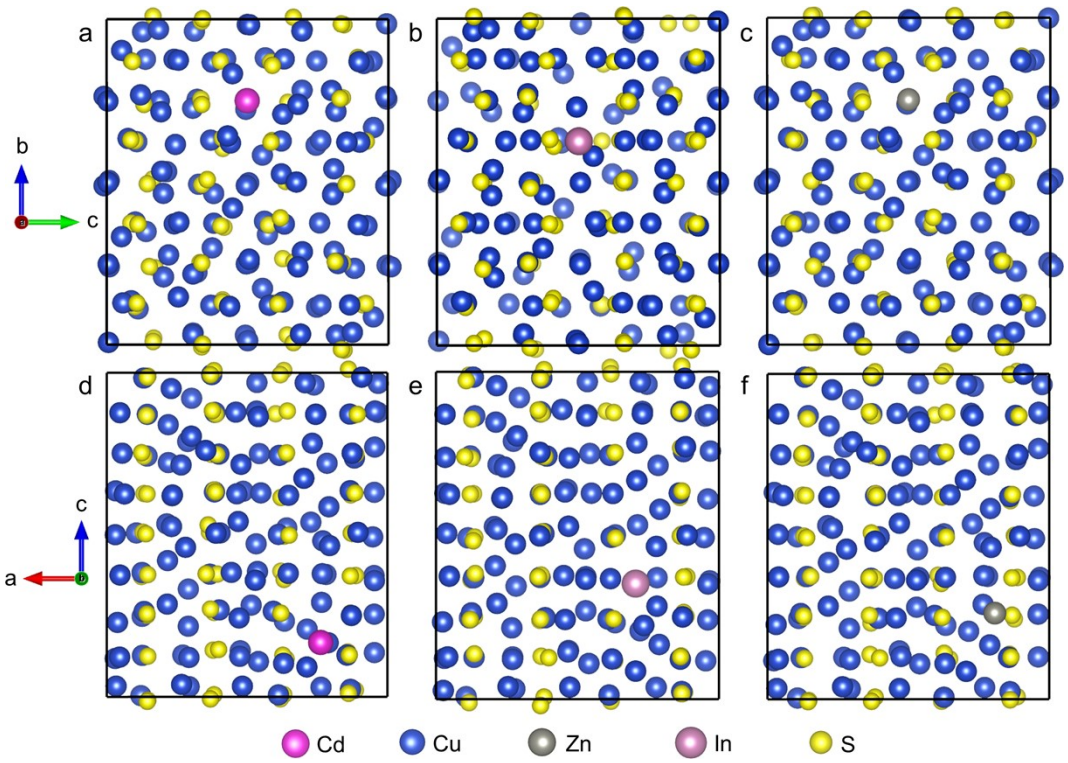

Fig. S6. The relaxed models for (a,d) Cd→$Cu_{1.81}S$, (b,e) In→$Cu_{1.81}S$ and (c,f) Zn→$Cu_{1.81}S$ reactions viewing along different directions. The black lines depict the unit cell of each crystal structure.

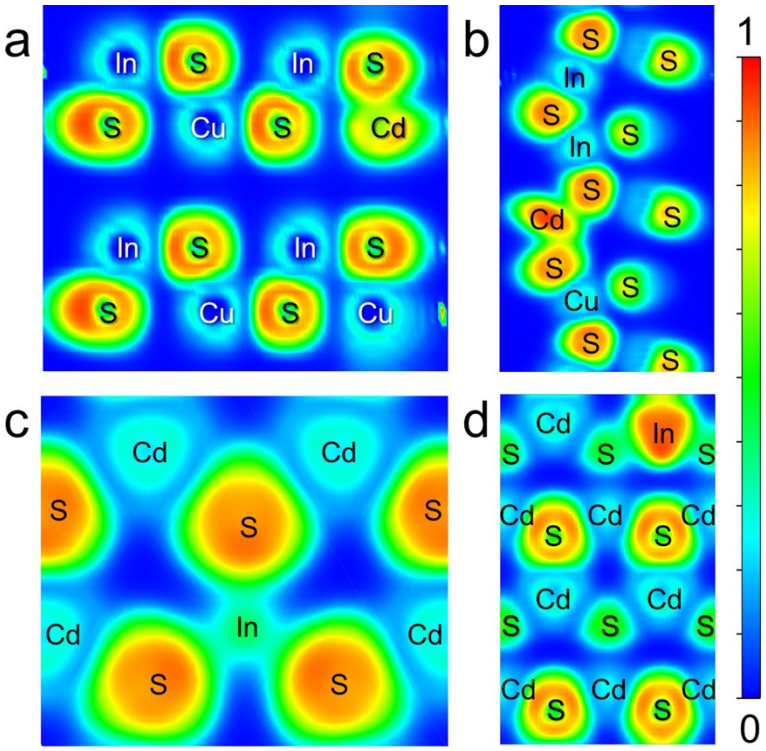

Fig. S7. (a,b) Sliced ELF of Cd→$CuInS_2$ reaction on (001) and (100) planes of $CuInS_2$, respectively. (c,d) Sliced ELF of In→CdS reaction on (001) and (100) planes of CdS, respectively.

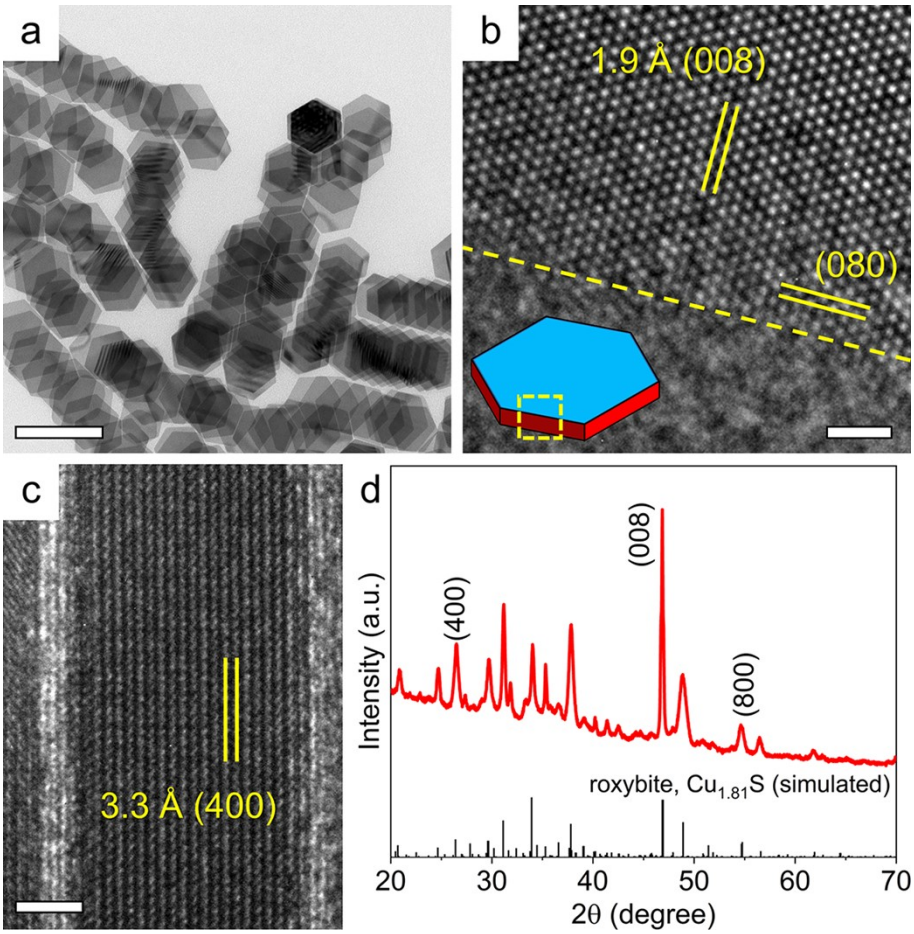

Fig. S8. (a) Low magnification TEM image, (b) top-view and (c) side-view HRTEM images, and (d) XRD pattern of roxbyite $Cu_{1.81}S$ nanoplates. Scale bars: (a) 200 nm, (b) 1 nm, (c) 2 nm.

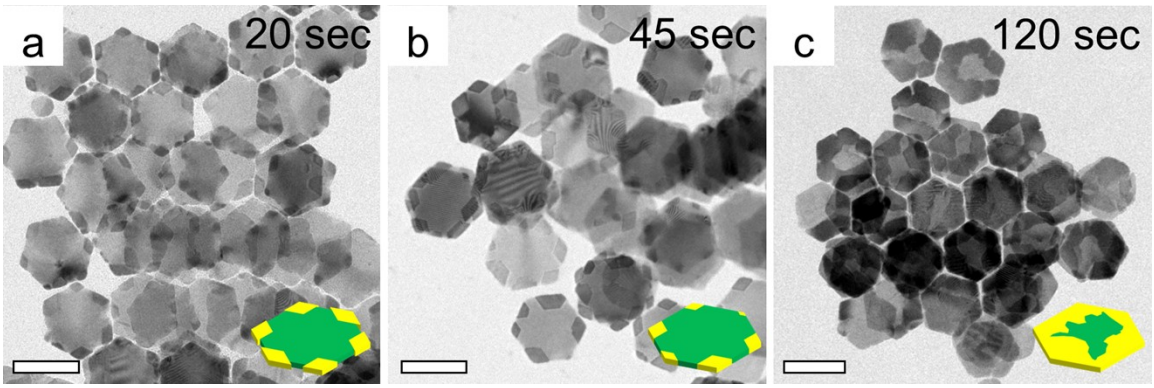

Fig. S9. TEM images of the reaction aliquots extracted at different reaction times of CE reaction of Cd^{2+} on $Cu_{1.81}S$ nanoplates.

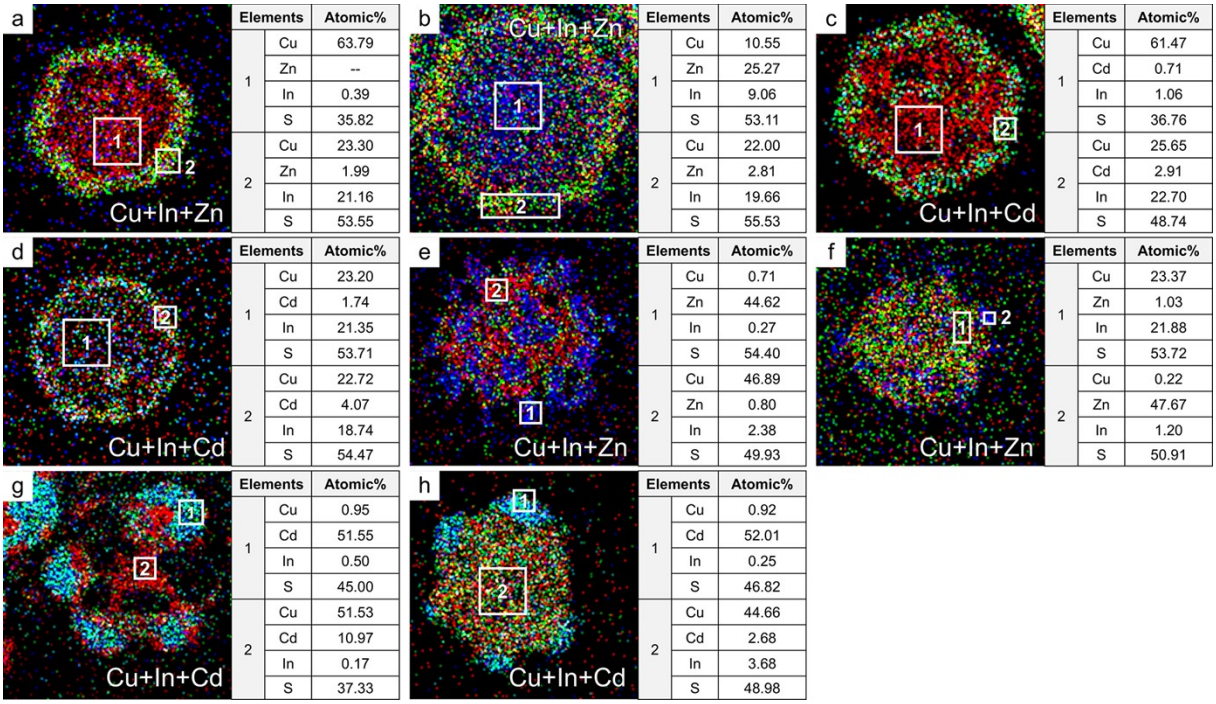

a	Elements	Atomic%
1	Cu	63.79
	Zn	--
	In	0.39
	S	35.82
2	Cu	23.30
	Zn	1.99
	In	21.16
	S	53.55

b	Elements	Atomic%
1	Cu	10.55
	Zn	25.27
	In	9.06
	S	53.11
2	Cu	22.00
	Zn	2.81
	In	19.66
	S	55.53

c	Elements	Atomic%
1	Cu	61.47
	Cd	0.71
	In	1.06
	S	36.76
2	Cu	25.65
	Cd	2.91
	In	22.70
	S	48.74

d	Elements	Atomic%
1	Cu	23.20
	Cd	1.74
	In	21.35
	S	53.71
2	Cu	22.72
	Cd	4.07
	In	18.74
	S	54.47

e	Elements	Atomic%
1	Cu	0.71
	Zn	44.62
	In	0.27
	S	54.40
2	Cu	46.89
	Zn	0.80
	In	2.38
	S	49.93

f	Elements	Atomic%
1	Cu	23.37
	Zn	1.03
	In	21.88
	S	53.72
2	Cu	0.22
	Zn	47.67
	In	1.20
	S	50.91

g	Elements	Atomic%
1	Cu	0.95
	Cd	51.55
	In	0.50
	S	45.00
2	Cu	51.53
	Cd	10.97
	In	0.17
	S	37.33

h	Elements	Atomic%
1	Cu	0.92
	Cd	52.01
	In	0.25
	S	46.82
2	Cu	44.66
	Cd	2.68
	In	3.68
	S	48.98

Fig. S10. Collection of overlapped elemental maps of different heterostructures. The quantitative EDS results are acquired from the area in the white box.

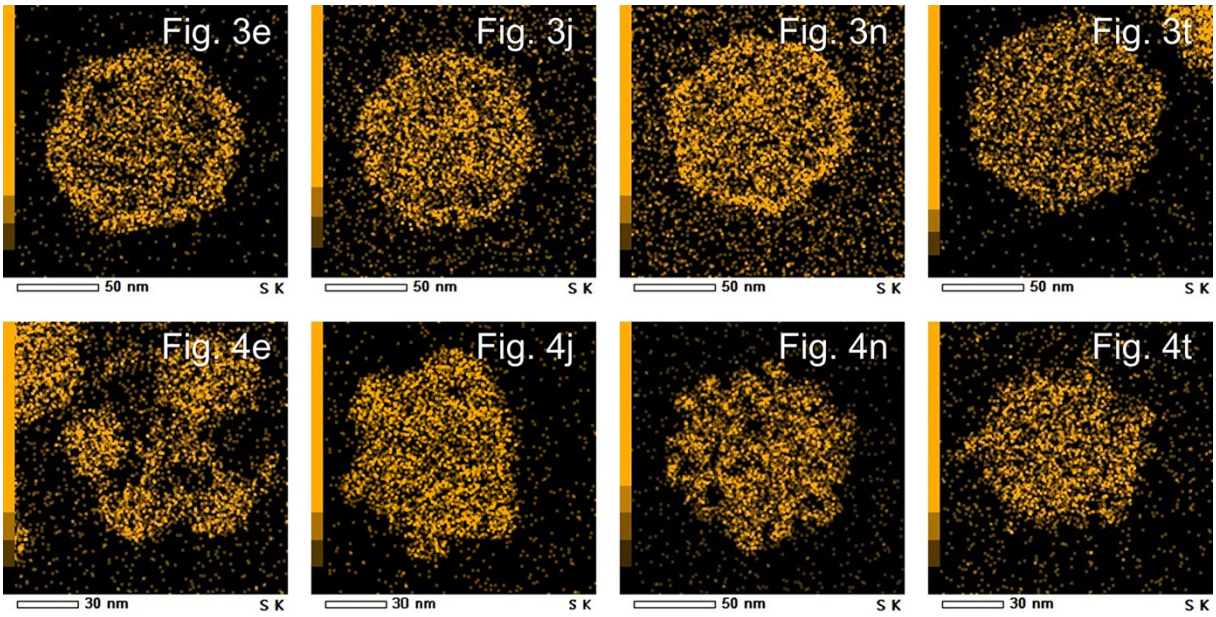

Fig. S11. Sulfur elemental maps discussed in the manuscript as noted.

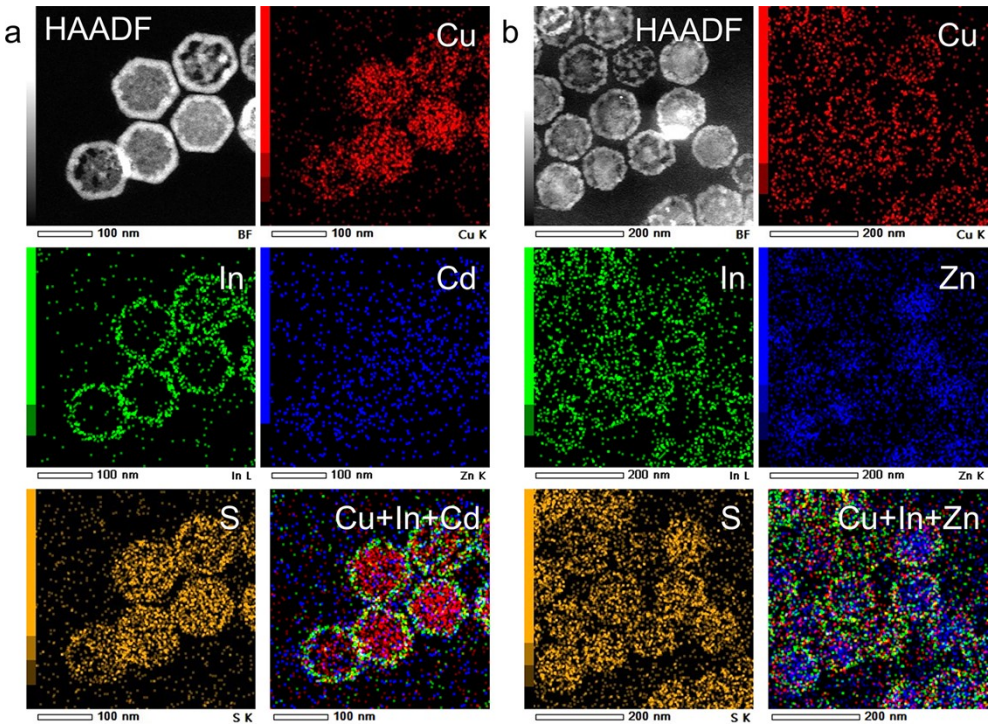

Fig. S12. Additional HAADF-STEM image and corresponding elemental maps of $Cu_{2-x}S@CuInS_2$ heterostructure nanoplates after Zn^{2+} exchange reaction at (a) 55 °C and (b) 155 °C.

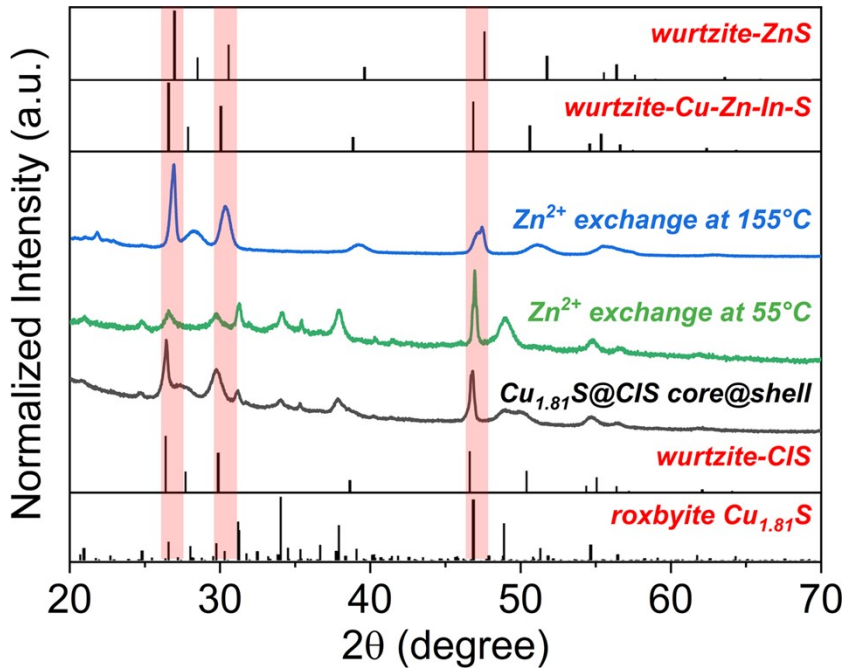

Fig. S13. XRD patterns of $Cu_{2-x}S$@$CuInS_2$ heterostructure nanoplates and products after Zn^{2+} exchange reaction at 55 °C and 155 °C.

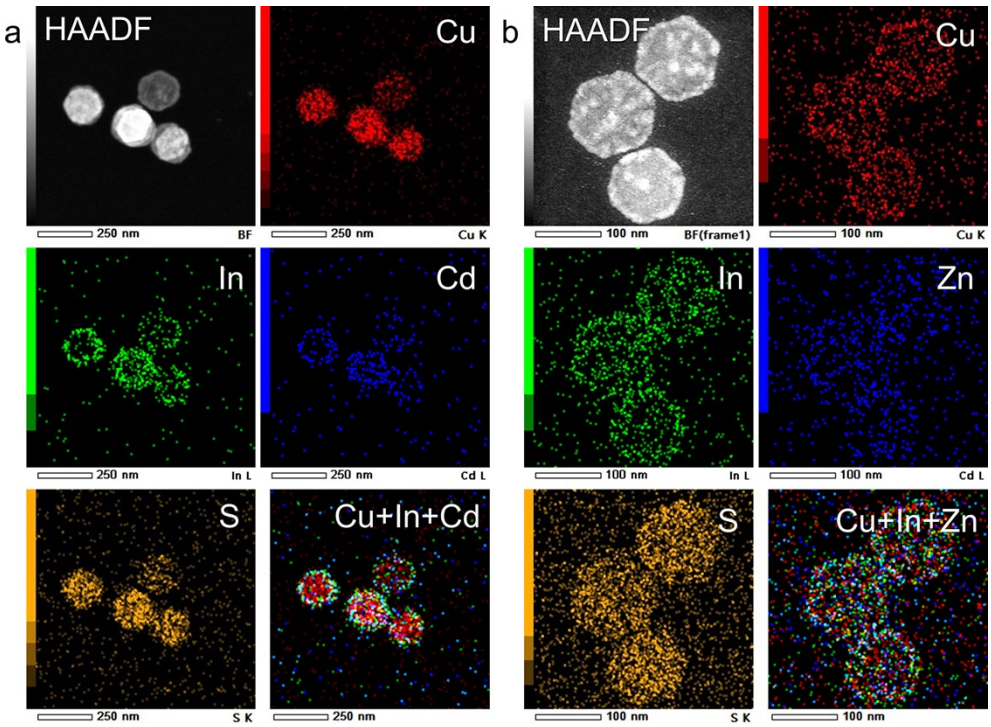

Fig. S14. Additional HAADF-STEM image, and corresponding elemental maps of $Cu_{2-x}S$@$CuInS_2$ heterostructure nanoplates after Cd^{2+} exchange reaction at (a) 55 °C and (b) 155 °C.

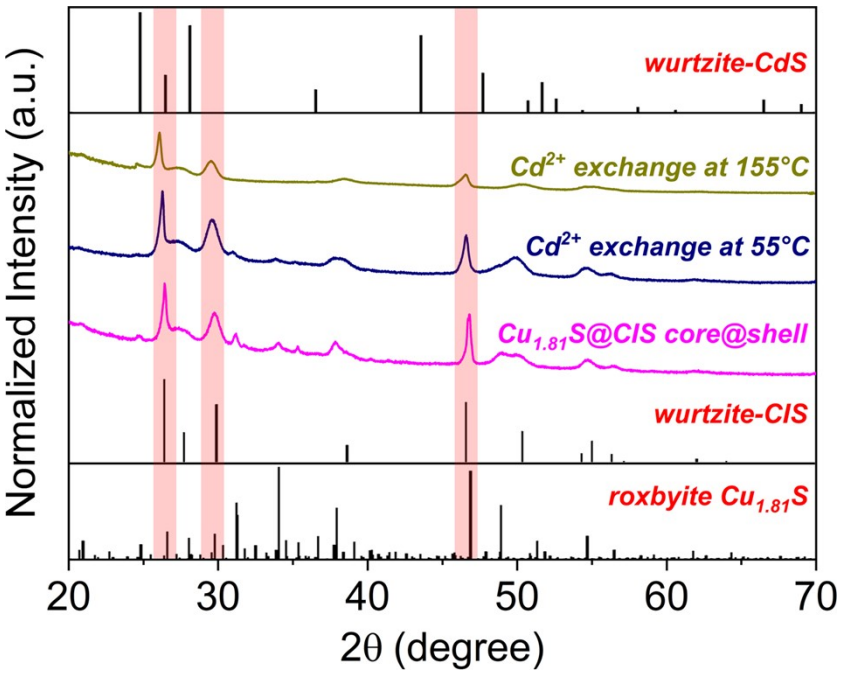

Fig. S15. XRD patterns of $Cu_{2-x}S$@$CuInS_2$ heterostructure nanoplates and products after Cd^{2+} exchange reaction at 55 °C and 155 °C.

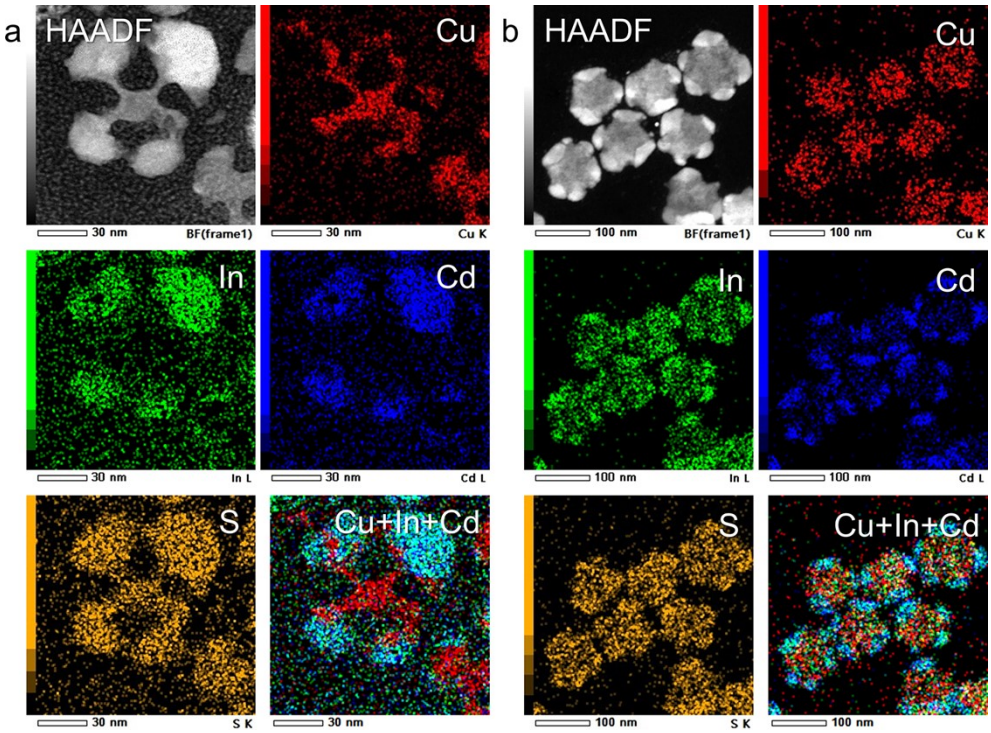

Fig. S16. Additional HAADF-STEM image, and corresponding elemental maps of $Cu_{2-x}S$/CdS heterostructure nanoplates after In^{3+} exchange reaction at (a) 55 °C and (b) 155 °C.

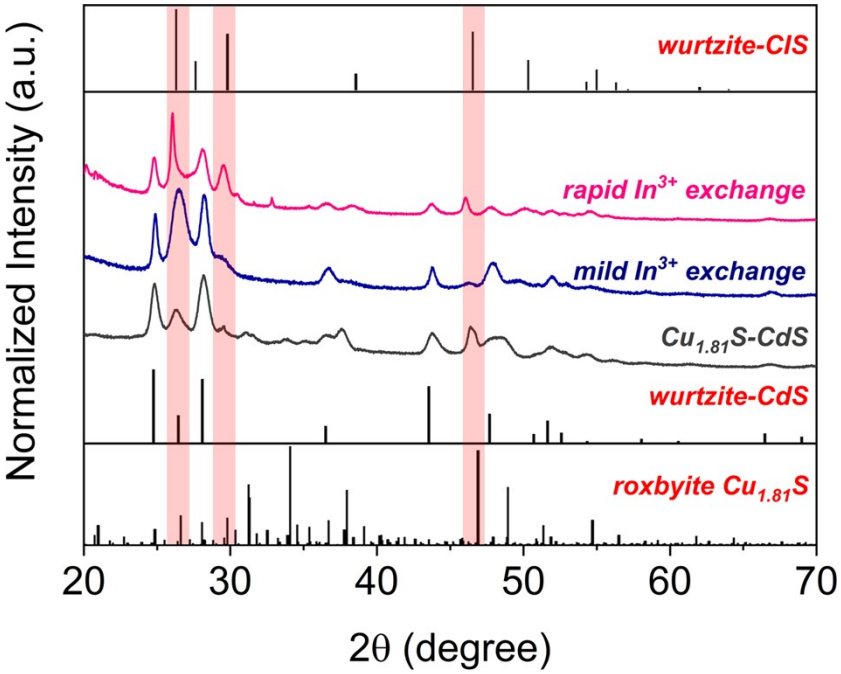

Fig. S17. XRD patterns of $Cu_{2-x}S$/CdS heterostructure nanoplates after In^{3+} exchange reaction at (a) 55 °C and (b) 155 °C.

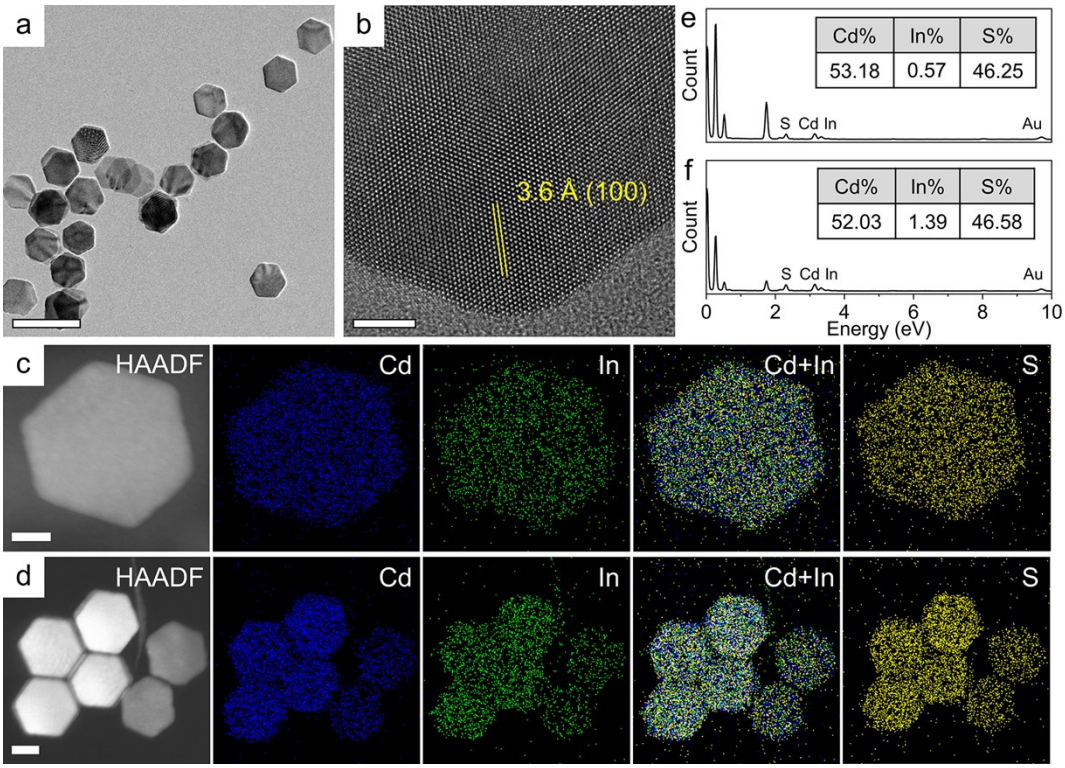

Fig. S18. (a) TEM and (b) HRTEM images of In exchange on CdS nanoplates at 55 °C. (c,d) HAADF and corresponding elemental maps for Cd, In and S. (e,f) EDS spectra and corresponding atomic ratio of Cd, In, and S for the EDS mapping of (c,d). Scale bars: (a) 200 nm, (b) 5 nm, (c) 25 nm, (d) 50 nm.

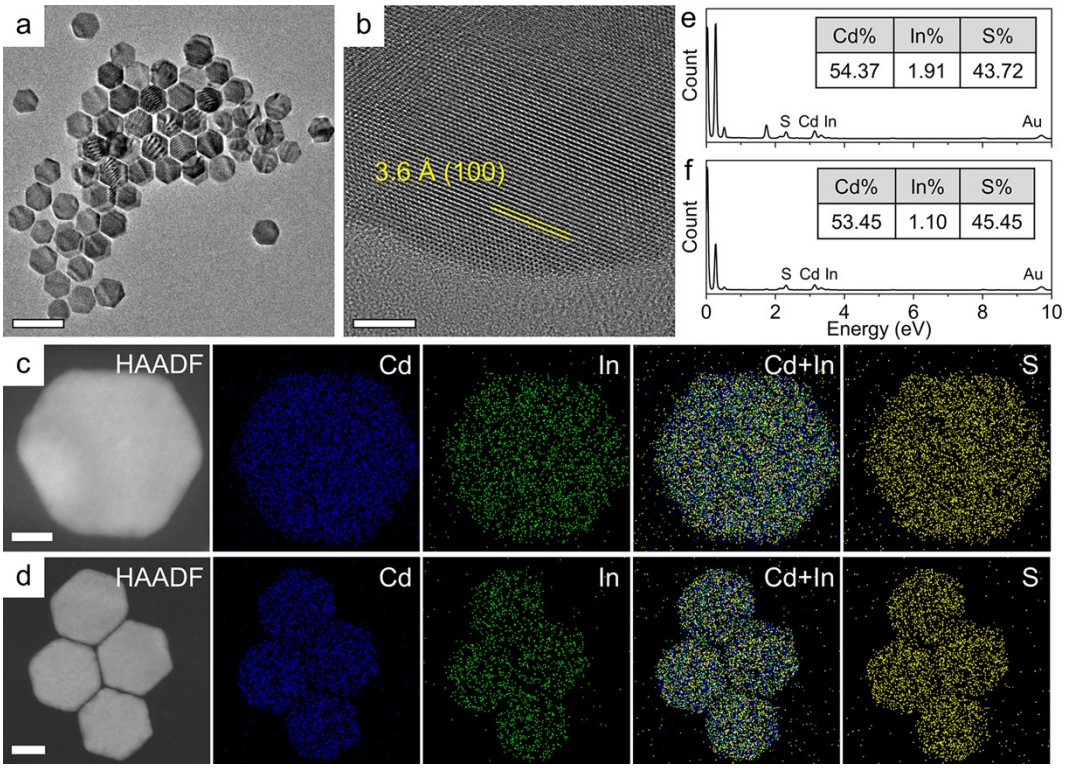

Fig. S19. (a) TEM and (b) HRTEM images of In exchange on CdS nanoplates at 155 °C. (c,d) HAADF and corresponding elemental maps for Cd, In and S. (e,f) EDS spectra and corresponding atomic ratio of Cd, In, and S for the EDS mapping of (c,d). Scale bars: (a) 200 nm, (b) 5 nm, (c) 25 nm, (d) 50 nm.

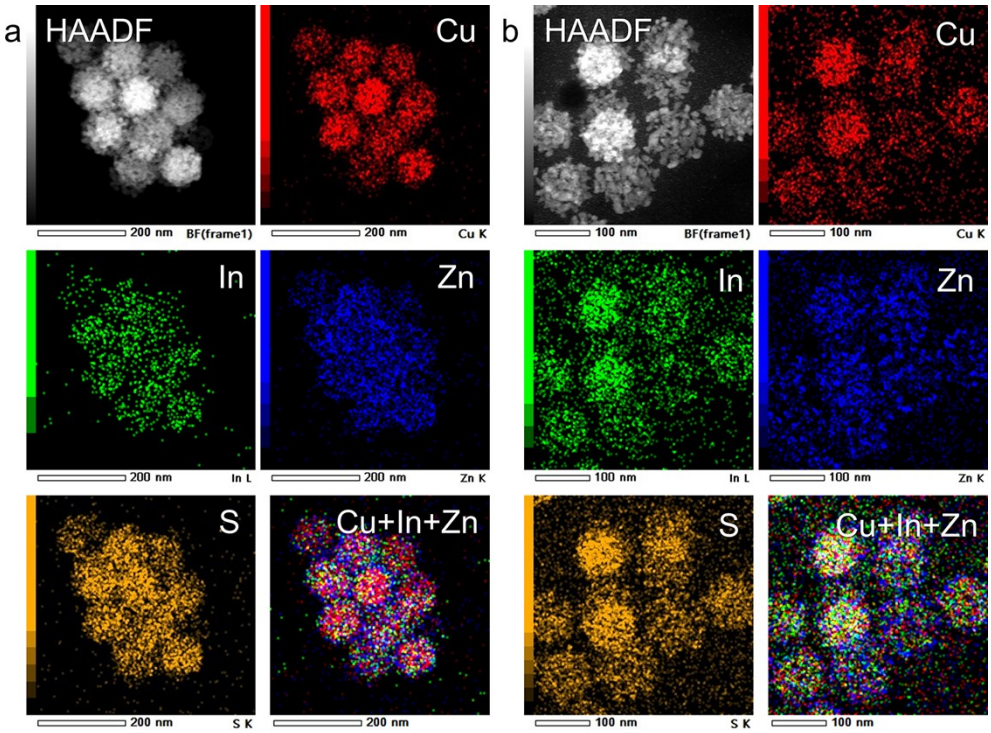

Fig. S20. Additional HAADF-STEM image, and corresponding elemental maps of $Cu_{2-x}S$/ZnS heterostructure nanoplates after In^{3+} exchange reaction at (a) 55 °C and (b) 155 °C.

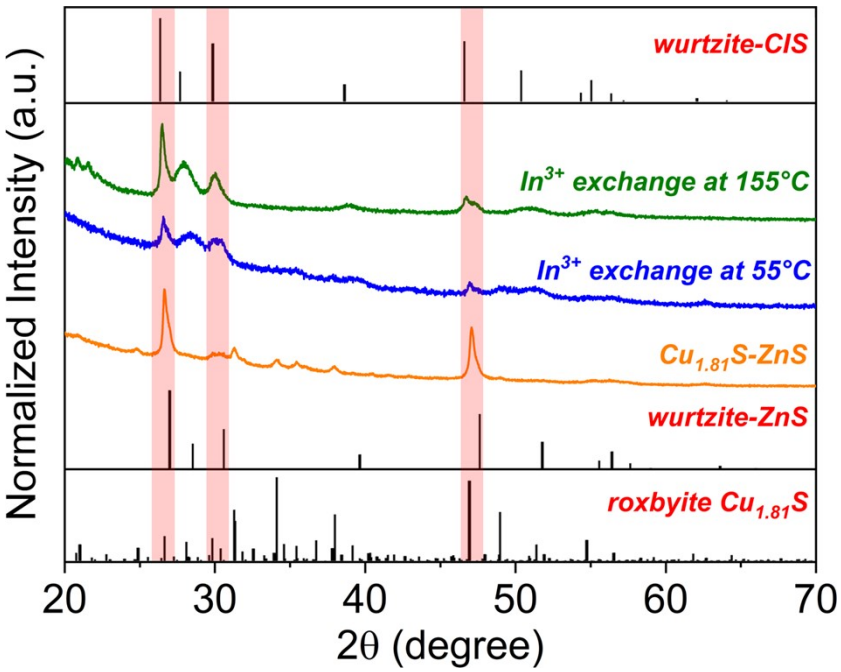

Fig. S21. XRD patterns of $Cu_{2-x}S$/ZnS heterostructure nanoplates after In^{3+} exchange reaction at (a) 55 °C and (b) 155 °C.

References:

1. Regulacio, M. D.; Ye, C.; Lim, S. H.; Bosman, M.; Polavarapu, L.; Koh, W. L.; Zhang, J.; Xu, Q. H.; Han, M. Y., One-Pot Synthesis of $Cu_{1.94}S$-CdS and $Cu_{1.94}S$-$Zn_xCd_{1-x}S$ Nanodisk Heterostructures. *J. Am. Chem. Soc.* **2011,** *133* (7), 2052-2055.

2. Lee, S.; Baek, S.; Park, J. P.; Park, J. H.; Hwang, D. Y.; Kwak, S. K.; Kim, S. W., Transformation from $Cu_{2-x}S$ Nanodisks to $Cu_{2-x}S$@$CuInS_2$ Heteronanodisks via Cation Exchange. *Chem. Mater.* **2016,** *28* (10), 3337-3344.

3. Fenton, J. L.; Steimle, B. C.; Schaak, R. E., Tunable Intraparticle Frameworks for Creating Complex Heterostructured Nanoparticle Libraries. *Science* **2018,** *360* (6388), 513-517.

4. Kresse, G.; Joubert, D., From Ultrasoft Pseudopotentials to the Projector Augmented-Wave Method. *Phys. Rev. B* **1999,** *59* (3), 1758-1775.

5. Kresse, G.; Furthmuller, J., Efficient Iterative Schemes for Ab Initio Total-Energy Calculations Using a Plane-Wave Basis Set. *Phys. Rev. B* **1996,** *54* (16), 11169-11186.

6. Perdew, J. P.; Burke, K.; Ernzerhof, M., Generalized Gradient Approximation Made Simple. *Phys. Rev. Lett.* **1996,** *77* (18), 3865-3868.

7. Horani, F.; Lifshitz, E., Unraveling the Growth Mechanism Forming Stable γ-In_2S_3 and β-In_2S_3 Colloidal Nanoplatelets. *Chem. Mater.* **2019,** *31* (5), 1784-1793.

8. Zhang, M.; Wang, Y. A.; Wang, X.; Zhao, B.; Ruan, W. D., Surface-Enhanced Raman Scattering (SERS) on Indium-Doped CdO (ICO) Substrates: A New Charge-Transfer Enhancement Contribution from Electrons in Conduction Bands. *J. Phys. Chem. C* **2021,** *125* (31), 17125-17132.

9. Liang, X. Y.; Ren, Y. P.; Bai, S.; Zhang, N.; Dai, X. L.; Wang, X.; He, H. P.; Jin, C. H.; Ye, Z. Z.; Chen, Q.; Chen, L. W.; Wang, J. P.; Jin, Y. Z., Colloidal Indium-Doped Zinc Oxide Nanocrystals with Tunable Work Function: Rational Synthesis and Optoelectronic Applications. *Chem. Mater.* **2014,** *26* (17), 5169-5178.

10. Wu, C.; Jiang, C.; Wang, X.; Ding, H.; Ju, H.; Zhang, L.; Chen, T.; Zhu, C., Interfacial Engineering by Indium-Doped CdS for High Efficiency Solution Processed $Sb_2(S_{1-x}Se_x)_3$ Solar Cells. *ACS Appl. Mater. Interfaces* **2019,** *11* (3), 3207-3213.

11. Della Gaspera, E.; Griggs, J.; Ahmed, T.; Walia, S.; Mayes, E. L. H.; Calzolari, A.; Catellani, A.; van Embden, J., Augmented Band Gap Tunability in Indium-Doped Zinc Sulfide Nanocrystals. *Nanoscale* **2019,** *11* (7), 3154-3163.

12. Liu, Z.; Zhong, Y.; Shafei, I.; Borman, R.; Jeong, S.; Chen, J.; Losovyj, Y.; Gao, X.; Li, N.; Du, Y.; Sarnello, E.; Li, T.; Su, D.; Ma, W.; Ye, X., Tuning infrared plasmon resonances in doped metal-oxide nanocrystals through cation-exchange reactions. *Nat. Commun.* **2019,** *10* (1), 1394.